New Journal of Physics
The open-access journal for physics

Absolute instruments and perfect imaging in geometrical optics

Tomáš Tyc[1], **Lenka Herzánová, Martin Šarbort and Klaus Bering**
Institute of Theoretical Physics and Astrophysics, Masaryk University,
Kotlářská 2, 61137 Brno, Czech Republic
E-mail: tomtyc@physics.muni.cz

New Journal of Physics **13** (2011) 115004 (23pp)
Received 30 June 2011
Published 8 November 2011
Online at http://www.njp.org/
doi:10.1088/1367-2630/13/11/115004

Abstract. We investigate imaging by spherically symmetric absolute instruments that provide perfect imaging in the sense of geometrical optics. We derive a number of properties of such devices, present a general method for designing them and use this method to propose several new absolute instruments, in particular a lens providing a stigmatic image of an optically homogeneous region and having a moderate refractive index range.

[1] Author to whom any correspondence should be addressed.

Contents

1. Introduction

In the last decade, perfect imaging became one of the hot topics in optics. This was triggered by a discovery of Sir J Pendry [1] who showed that a slab of material with negative refractive index can focus light on a spot much smaller than the wavelength of light. Modern metamaterials with carefully designed electric and magnetic responses [2] provided a suitable experimental background for testing such super-resolution [3], but it has turned out that there are severe limitations due to strong absorption in negatively refracting materials [4]. This started a search for other devices that could provide super-resolution but would not suffer from the disadvantages related to negative refraction. It has turned out recently that such devices do exist, which was demonstrated both theoretically [5, 6] and experimentally [7] for a well-known optical device, Maxwell's fish eye [8]. Optical imaging with super-resolution is generally called perfect imaging and the corresponding devices are called perfect lenses.

The concept of perfect imaging has become important also in geometrical optics where limitations of optical instruments are of a different kind. There, the diffraction limit of resolution is not the subject of investigation, but instead one seeks to minimize or even eliminate the optical aberrations of the device. Remarkably, there exist devices in which this elimination can be made perfect; they are called absolute instruments [9]. An important subset of absolute instruments is formed by devices that produce images geometrically similar to the imaged objects. Within geometrical optics, such images are called perfect [9]. Hence, the meaning of 'perfect imaging' is different in geometrical and in wave optics. In particular, an imaging device that is perfect from the point of view of geometrical optics may or may not be perfect from the point of view of

wave optics and vice versa. The only devices that are known to produce images perfect in both senses are Pendry's slab [1] and Maxwell's fish eye surrounded by a mirror [5, 7]; it remains unknown as to whether other lenses producing stigmatic images also provide super-resolution. However, as the answer is very likely to be positive, a search for new absolute instruments with interesting and useful properties is highly desirable, because such devices might provide unprecedented resolution and find applications in imaging or lithography.

In this paper, we focus on absolute instruments and perfect imaging from the point of view of geometrical optics. We analyse the general properties of imaging by spherically symmetric absolute instruments and develop a method for designing such devices. We then use this method for proposing several devices with interesting properties.

The paper is organized as follows. In section 2, we analyse spherically symmetric absolute instruments and derive several general results. In section 3, we solve the inverse scattering problem for spatially confined rays and based on this result we develop a method for designing absolute instruments in section 4. In section 5, we give some simple examples of absolute instruments and in sections 6 and 7 we discuss devices with homogeneous regions and multiple image points, respectively. We conclude in section 8.

2. Properties of spherically symmetric absolute instruments

In this paper, we will consider isotropic spherically symmetric refractive index profiles $n(r)$. Such situations have a great advantage: if some point at radius r is imaged stigmatically, then the same is true for all points at the same radius. At the same time, usually the object to be imaged must be embedded directly into the optical medium and the rays emerge in all directions from the object and come from all directions to the image. This is quite different from the usual imaging, e.g. by a camera or a telescope where rays propagate more or less in one direction.

2.1. Angular momentum and turning parameter

It is well known (and follows, for example, from the analogy between geometrical optics and classical mechanics) that in spherically symmetrical refractive index profiles $n(r)$ light rays propagate in a plane containing the centre of symmetry. This is a consequence of conservation of the quantity analogous to mechanical angular momentum, the magnitude of which is [9]

$$L = rn(r)\sin\alpha, \tag{1}$$

where α is the angle between the tangent to the particle trajectory and the radius vector. Motion in spherically symmetric index distributions $n(r)$ is therefore effectively two dimensional (2D), and we will treat it as such unless otherwise stated.

For a spherically symmetric medium, an important role is played by the radially normalized index function

$$N(r) = rn(r), \tag{2}$$

which is also known as the turning parameter [10, 11]. Consider a light ray propagating with angular momentum L. It follows from equations (1) and (2) that $L = N(r)\sin\alpha$ and hence the ray can propagate only in the regions where $L \leqslant N(r)$. When it gets to the point where $L = N(r)$, then $\alpha = \pi/2$ and the ray propagates purely in the angular direction. Such a point is called a turning point.

2.2. Stigmatic images and absolute instruments

According to *Principles of Optics* by M Born and E Wolf [9], an absolute instrument is a device that images stigmatically a 3D domain of space. A stigmatic image of a point A is point B through which an infinity of rays emerging from A pass.

We shall distinguish between two cases of a stigmatic image. In the first case, the image of a point A is formed at B by all rays emerging from A into some nonzero solid angle. We shall then call B a *strong stigmatic image* (or simply *strong image*) of A. In the second case, although there is an infinite number of rays going from A to B, these rays constitute just a zero solid angle. Then we shall call B a *weak (stigmatic) image*. For example, a cylindrical lens can form a whole line of weak images of a given point but no strong image.

2.3. Mutual position of an object and its image

Suppose we have an absolute instrument with refractive index $n(r)$ that stigmatically images a point A with radial coordinate r_A to a point B with radial coordinate r_B. This means that an infinite number of rays emerging from A meet at B [9]. Imagine we shift the point A infinitesimally in the angular direction by an angle $\mathrm{d}\varphi$ to a new position A′ separated from A by distance $r_\mathrm{A}\mathrm{d}\varphi$. From the spherical symmetry it follows that the image B gets shifted by the same angle $\mathrm{d}\varphi$ to a new position B′ separated from B by $r_\mathrm{B}\mathrm{d}\varphi$. Now Maxwell's theorem for absolute instruments [9] states that the optical length of any curve and of its image is the same, which we can apply to the lines AA′ and BB′. Cancelling the angle $\mathrm{d}\varphi$, we obtain

$$n(r_\mathrm{A})\, r_\mathrm{A} = n(r_\mathrm{B})\, r_\mathrm{B}. \tag{3}$$

Assuming that we shift the point A in the radial direction by $|\mathrm{d}r_\mathrm{A}|$ to a point A″ instead, the point B is also shifted in the radial direction to the point B″. This follows from the fact that imaging by absolute instruments is conformal [9], another consequence of Maxwell's theorem: if the angle A′AA″ is $\pi/2$, so must be the angle B′BB″. From Maxwell's theorem applied to the lines AA″ and BB″, we then obtain

$$n(r_\mathrm{A})|\mathrm{d}r_\mathrm{A}| = n(r_\mathrm{B})|\mathrm{d}r_\mathrm{B}|. \tag{4}$$

Dividing equation (4) by (3), we obtain

$$\frac{\mathrm{d}r_\mathrm{A}}{r_\mathrm{A}} = \pm\frac{\mathrm{d}r_\mathrm{B}}{r_\mathrm{B}} \tag{5}$$

with the solutions

$$r_\mathrm{B} = k r_\mathrm{A}, \tag{6}$$

$$r_\mathrm{B} = \frac{k}{r_\mathrm{A}}, \tag{7}$$

corresponding to plus and minus sign in equation (5), respectively, and an integration constant $k > 0$.

Another question is related to the mutual angular position of an object and its image. Can there be a situation that object A, its strong stigmatic image B and the origin O (centre of symmetry of the lens) do not lie on a single straight line? Imagine such a situation. Since B is a strong image of A, a full solid angle of rays starting from A pass through B. We can rotate

these rays around the line OA by some angle φ, which also moves the point B to a new position B′. The rotated rays now pass through B′ which, due to the spherical symmetry of the lens, must also be a strong stigmatic image of A. This would mean that A has strong images along the whole circle that is obtained by rotation of point B around the axis OA, which is clearly impossible. So we must conclude that points A, B and O lie on a single straight line. This way image B is either on exactly the same side of O as is A or on exactly the opposite side.

Note that this argument is not valid in two dimensions where the mutual position of a point and its image in a rotationally symmetric absolute instrument is less restricted. For the same reason, this argument is not valid in 3D for weak images.

2.4. Value of the constant k in equation (6)

An interesting question is related to the possible values of the constant k in equation (6). We conjecture that the only possibility is $k = 1$. Although we have not been able to show this in the completely general situation, the proof can be given in two practically important cases. For the first case, assume that the constant k is the same for all the points that are imaged by the lens. But if B is an image of A, then also A is an image of B, so $r_A = kr_B$ must also hold along with equation (6), from which then $k = 1$ follows.

The assumption of the second case is that among the rays that contribute to the image B of point A there is also the ray for which A is a turning point. In other words, we assume that a ray starting from point A in the angular direction makes it to the image of A formed at point B. Since equation (3) can be rewritten as $N(r_A) = N(r_B)$, it follows that point B is a turning point for the same ray as well. Next we use equation (5) with the plus sign from which equation (6) has been derived, i.e. $dr_A/r_A = dr_B/r_B$. From this equation combined with $N(r_A) = N(r_B)$ then follows:

$$r_A \frac{dN(r_A)}{dr_A} = r_B \frac{dN(r_B)}{dr_B}. \tag{8}$$

We see that the derivative dN/dr has the same sign at both r_A and r_B. However, if $k \neq 1$, this is a contradiction with the fact that the same ray has its turning points at A as well as B. To see this, suppose that $k > 1$ (in the opposite case we can relabel the points A and B), and so $r_B > r_A$. Then if the derivative dN/dr is negative at $r = r_A$, then for the ray with angular momentum $L = N(r_A)$ the region $r > r_A$ is inaccessible because in this region $L > N(r)$, which is impossible, and so the ray cannot make it to B. On the other hand, if the derivative dN/dr is positive at $r = r_A$, then it is also positive at $r = r_B$. For a similar reason then the ray with angular momentum $L = N(r_A) = N(r_B)$ cannot make it to A, which is a contradiction. Hence, the only possibility is $r_A = r_B$, which then implies $k = 1$.

We thus see that there are just two cases of imaging by spherically symmetric absolute instruments: either the image is given by spherical inversion (since $r_A r_B = k$) of the object, possibly combined with some rotation, or it is congruent with it. We have arrived at a slightly stronger statement than that derived in [9] for absolute instruments in general. We will see in section 4 that equation (7) corresponds to the generalized Maxwell's fish eye; all other spherically symmetric absolute instruments correspond to equation (6) with $k = 1$, and so they give images congruent with the object and their magnification is unity. This means that the imaging by such a device is perfect in the sense of geometrical optics [9].

3. Inverse scattering problem for spatially confined rays

In the inverse scattering problem in mechanics, the task is to determine an unknown potential from the scattering angle, which is a known (e.g. measured) function of the impact parameter. The problem was solved for central potentials in 1953 by Firsov [12] and the analogous problem in optics was solved by Luneburg [13]. In the situations considered there, the particle or light ray is incident from infinity, undergoes scattering and leaves for infinity again, and so the motion is not spatially confined. However, the situation where the motion is restricted to a finite region of space may be equally important for the design of absolute instruments and perfect lenses. The inverse problem can be formulated and solved also in this case; the solution for mechanical motion was given without derivation by Ostrovsky in [14]. In the following, we derive the inversion formula for confined motion in the optical case.

To derive the inversion formula, we will assume that the function $N : r \mapsto N(r)$ in equation (2) is increasing for $r \leqslant r_0$ and decreasing for $r \geqslant r_0$ with some radius $r_0 > 0$. (There are obviously more general profiles $N(r)$ and the inverse problem can be solved for them as well, but we will not consider them here.) Then the function $N(r)$ has a global maximum $L_0 \equiv \max N = N(r_0)$ at the point $r = r_0$. The inverse function $r : N \mapsto r(N)$ is multi-valued, i.e. has two branches $r_\pm$. One branch $r_- : N \mapsto r_-(N)$ maps into the inner region $[0, r_0]$, and the other branch $r_+ : N \mapsto r_+(N)$ maps into the outer region $[r_0, \infty)$. In this case, we can invert the inequality $L \leqslant N(r)$ into a double inequality

$$r_-(L) \leqslant r \leqslant r_+(L), \tag{9}$$

which explicitly specifies the allowed confined region. In other words, for angular momentum $L < L_0$, there are two turning points $r_\pm(L)$. Moreover, a light ray with angular momentum $L = L_0$ will propagate along a circular trajectory with radius r_0, while angular momentum $L > L_0$ is forbidden.

For the subsequent calculations, it turns out to be more convenient to work in terms of a new coordinate $x = \ln r$ rather than the radius r. We will also introduce corresponding notation $x_\pm = \ln r_\pm$, $x_0 = \ln r_0$, etc, in the obvious fashion. At a general point of a ray trajectory, the derivative of the polar angle φ is

$$\frac{\mathrm{d}\varphi}{\mathrm{d}x} = r\frac{\mathrm{d}\varphi}{\mathrm{d}r} = \tan\alpha = \frac{L}{\sqrt{N^2(r) - L^2}}, \tag{10}$$

where we have used that $L = N(r)\sin\alpha$. With the help of equation (10), the increment of the polar angle corresponding to motion between $r_-(L)$ and $r_+(L)$ can be written as

$$\Delta\varphi(L) = L\int_{r_-(L)}^{r_+(L)} \frac{\mathrm{d}r}{r\sqrt{N^2(r) - L^2}} = L\int_{x_-(L)}^{x_+(L)} \frac{\mathrm{d}x}{\sqrt{N^2(x) - L^2}}. \tag{11}$$

We shall call $\Delta\varphi$ the turning angle; it expresses the change of the ray direction between two consequent turning points.

The task of the inverse scattering problem is to find the refractive index $n(r)$ (or equivalently, the function $N(x)$) from the known turning angle $\Delta\varphi(L)$. It can be solved in a way similar to finding the 1D potential from the known period of oscillations as a function of energy [15]. We divide $\Delta\varphi(L')$ by $\sqrt{L'^2 - L^2}$, where L' is an integration parameter, and

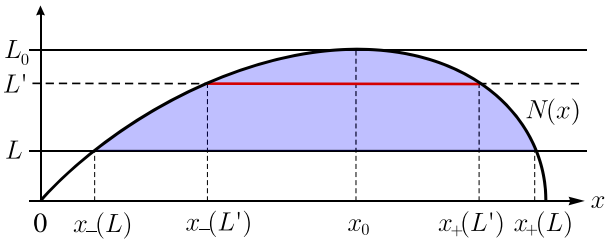

Figure 1. The change of integration limits in equation (12) illustrating that $\int_L^{L_0}\int_{x_-(L')}^{x_+(L')} u(x,L')\,\mathrm{d}x\,\mathrm{d}L' = \int_{x_-(L)}^{x_+(L)}\int_L^{N(x)} u(x,L')\,\mathrm{d}L'\,\mathrm{d}x$.

integrate with respect to L' from L to L_0:

$$\begin{aligned}\int_L^{L_0}\frac{\Delta\varphi(L')\,\mathrm{d}L'}{\sqrt{L'^2-L^2}} &\overset{(11)}{=} \int_L^{L_0}\int_{x_-(L')}^{x_+(L')}\frac{\mathrm{d}x}{\sqrt{N^2(x)-L'^2}}\frac{L'\,\mathrm{d}L'}{\sqrt{L'^2-L^2}}\\ &= \int_{x_-(L)}^{x_+(L)}\int_L^{N(x)}\frac{L'\,\mathrm{d}L'}{\sqrt{L'^2-L^2}}\frac{\mathrm{d}x}{\sqrt{N^2(x)-L'^2}}\\ &= \int_{x_-(L)}^{x_+(L)}\left[\arcsin\sqrt{\frac{L'^2-L^2}{N^2(x)-L^2}}\right]_{L'=L}^{L'=N(x)}\mathrm{d}x\\ &= \int_{x_-(L)}^{x_+(L)}\left(\frac{\pi}{2}-0\right)\mathrm{d}x = \frac{\pi}{2}\left(x_+(L)-x_-(L)\right), \end{aligned} \tag{12}$$

where we have inverted the order of integration and changed the integration limits appropriately; see figure 1. Equation (12) yields the inversion formula

$$\ln\frac{r_+(L)}{r_-(L)} = \frac{2}{\pi}\int_L^{L_0}\frac{\Delta\varphi(L')\,\mathrm{d}L'}{\sqrt{L'^2-L^2}}, \tag{13}$$

which solves the inverse scattering problem. The mechanical equivalent of equation (13) was presented in [14] without derivation.

4. Method for designing absolute instruments

In the following, we will describe a general method for designing absolute instruments. This method was sketched in [14] but was not given explicitly. Consider the situation when the turning angle $\Delta\varphi$ is independent of L and equal to π/m, $m \in \mathbb{R}$. This is a practically important case; if, for instance, $m = p/q$ with p, q coprimes and p even, then the trajectory will be symmetric with respect to rotation by π around the origin in the plane of propagation. A strong stigmatic image of a point A at the position $\vec{r}$ will therefore be formed at $-\vec{r}$. If $m = p/q$ with p odd, a strong stigmatic image of a point A will be formed at A itself; the ray arrives there after encircling the origin q times. This will be shown in figure 5.

For $\Delta\varphi(L) = \pi/m$ we obtain from equation (13) $\ln[r_+(L)/r_-(L)] = (2/m)\,\mathrm{arcosh}\,(L_0/L)$, which can be expressed as

$$\frac{L_0}{L} = \frac{1}{2}\left[\left(\frac{r_+(L)}{r_-(L)}\right)^{m/2} + \left(\frac{r_-(L)}{r_+(L)}\right)^{m/2}\right]. \tag{14}$$

Now comes the key step of our derivation. We define a function $f(r)$ such that

$$f(r) = \begin{cases} r_+(N(r)), & \text{for} \quad r \leqslant r_0, \\ r_-(N(r)), & \text{for} \quad r \geqslant r_0. \end{cases} \tag{15}$$

The function $f(r)$ is hence defined such that for a given lower turning point r_- it produces the upper turning point r_+ corresponding to the same angular momentum and vice versa:

$$r_\pm = f(r_\mp). \tag{16}$$

We can say that the point r_+ is dual to the point r_- and vice versa. It also follows from this definition that applying the function f twice yields the original value, $f(f(r)) = r$, and therefore the graph of f is symmetric with respect to the axis of the first quadrant. The graph intersects this axis at the point $r_+ = r_- = r_0$, which corresponds to the circular ray trajectory.

With the function $f(r)$ defined this way, we can express L from equation (14) and either keep r_- and replace r_+ by $f(r_-)$ or keep r_+ and replace r_- by $f(r_+)$. Then taking advantage of the fact that $L = N$ at $r_\pm$ and omitting the index of $r_\pm$, we obtain

$$N(r) = 2L_0\left[\left(\frac{r}{f(r)}\right)^{m/2} + \left(\frac{f(r)}{r}\right)^{m/2}\right]^{-1}. \tag{17}$$

Finally, we express $n(r) = N(r)/r$ as

$$n(r) = \frac{2L_0}{r\left[\left(\frac{r}{f(r)}\right)^{m/2} + \left(\frac{f(r)}{r}\right)^{m/2}\right]}. \tag{18}$$

Equation (18) provides a powerful tool for designing absolute instruments. For any chosen function $f(r)$ satisfying the condition above and a suitable value of m it gives a refractive index profile with focusing properties, i.e. an absolute instrument. We will demonstrate this on several known examples first and then proceed to new devices.

5. Examples of absolute instruments

In all the following examples, we assign unit radius and unit refractive index to the circular ray, so $r_0 = L_0 = 1$. In the first example, the object and its image are related by spherical inversion, and in the other ones they are congruent, as discussed in section 2.

- *Generalized Maxwell's fish eye*
  Consider an absolute instrument in which the position of object and image is given by equation (7). Apparently, if r_A is a turning point, then r_B must also be a turning point, which leads to $r_+r_- = k = r_0^2 = 1$ (the case of a general k can be obtained easily by spatial scaling) and hence $f(r) = 1/r$. Then equation (18) yields

$$n(r) = \frac{2}{r^{1-m} + r^{m+1}}, \tag{19}$$

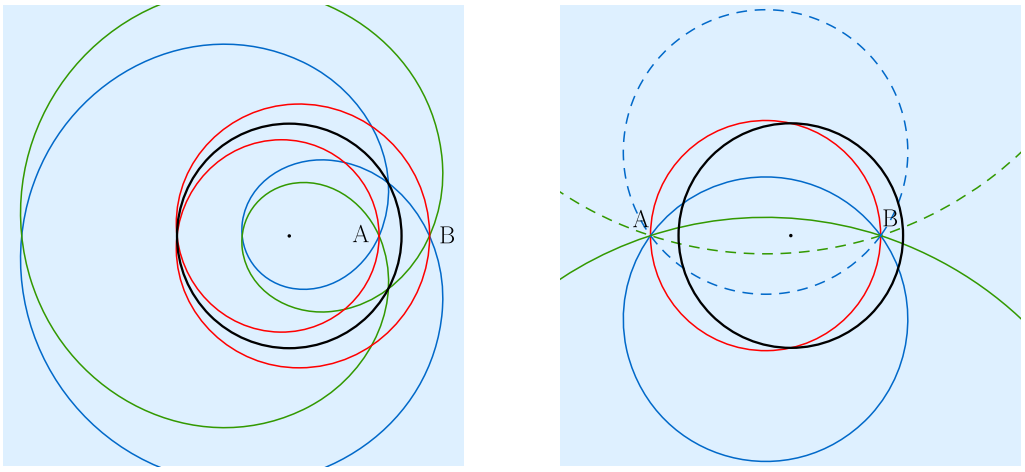

(a) (b)

Figure 2. Ray trajectories in (a) generalized Maxwell's fish eye with $m = 1/2$ and (b) Maxwell's fish eye. The source and its image are denoted by A and B, respectively. Here as well as in all subsequent figures, the black circle corresponds to the circular trajectory at $r = r_0$ with the maximum possible angular momentum L_0.

which is the generalized Maxwell's fish eye profile discussed in [16]. Light rays in this lens are shown in figure 2(a) for $m = 1/2$.
For $m = 1$, we obtain

$$n(r) = \frac{2}{1+r^2}, \tag{20}$$

which is the well-known Maxwell's fish eye refractive index profile [8]. The trajectories are circles intersecting the unit circle at two opposite points. Light rays are shown in figure 2(b).

- *Luneburg lens profile*
  Take $m = 2$ and $f(r) = \sqrt{2 - r^2}$. Then equation (18) yields

$$n(r) = \sqrt{2 - r^2}. \tag{21}$$

  For $r \leqslant 1$, this coincides with the well-known refractive index of Luneburg lens [13] which has, however, $n = 1$ for $r > 1$. The index (21) corresponds to the Hooke potential in mechanics and ray trajectories are ellipses centred at the origin [11]; see figure 3(a).

- *Eaton/Miñano lens profile*
  Take $m = 1$ and $f(r) = 2 - r$. Then equation (18) yields

$$n(r) = \sqrt{(2/r) - 1}. \tag{22}$$

  This is the well-known index profile of Eaton or Miñano lens [17, 18] which have, however, $n = 1$ for $r > 1$ or $r < 1$, respectively. The index (22) corresponds to elliptic motion in the Newton potential in mechanics and ray trajectories are confocal ellipses with focus at the origin and with the main semiaxes of unit length [11]; see figure 3(b).

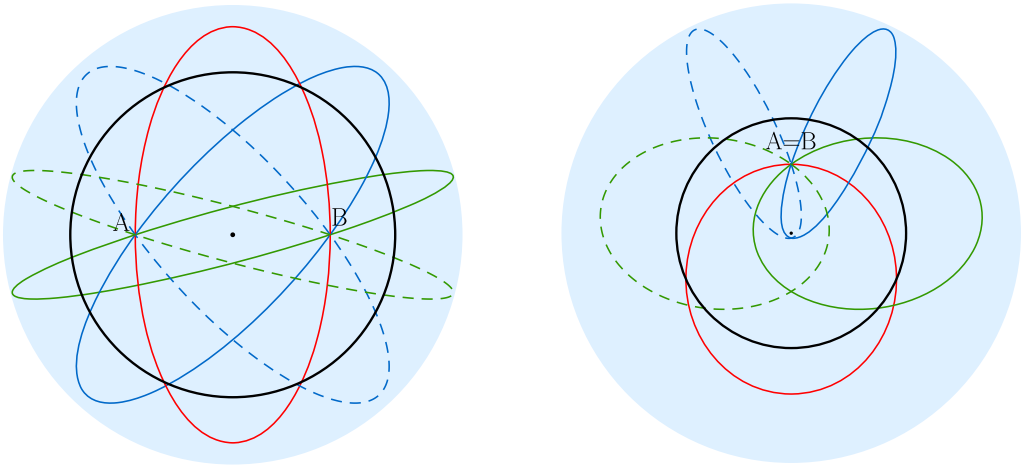

(a) (b)

Figure 3. Ray trajectories in the profile given by (a) equation (21) corresponding to Luneburg profile and (b) equation (22) corresponding to the Eaton/Miñano profile. The optical medium is shown in light blue; the refractive index reaches zero at the edge of the medium. In the Eaton/Miñano profile image B coincides with source A.

- *Maxwell's fish eye mirror*
  Take $m = 2$ and $f(r) = 1$ for $r < 1 = r_0$. From the symmetry of the function f it follows that it is undefined for $r \geqslant 1$; the rays cannot get beyond the unit circle, which means that they must be reflected there. Substituting into equation (18), we obtain for $r \in [0, 1)$ the index given by equation (20). This is the so-called Maxwell's fish eye mirror discussed in detail in [5] with rays as shown in figure 4.
- *Lenses generated by a sample function* $f(r)$
  To show the generality of our method, we choose some arbitrary function $f(r)$ with the restriction that it is symmetric with respect to the axis of the first quadrant. Let us choose

$$f(r) = \begin{cases} 3 - 2r, & \text{for} \quad r \leqslant 1, \\ (3 - r)/2, & \text{for} \quad r \geqslant 1, \end{cases} \tag{23}$$

  see its graph in figure 5(a). Using different values of m, we obtain different absolute instruments. The rays in some of them are shown in figures 5(b)–(d) for $m = 2$, $m = 5/2$ and $m = 2/3$.

5.1. Lenses with mirrors and index discontinuities

On the example of Maxwell's fish eye mirror, we have seen that an interval of r on which the function $f(r)$ from equation (16) was constant corresponded to a spherical mirror. As we will see, this is quite a general feature.

Consider the situation when the function $f(r)$ is constant and equal to $c \geqslant r_0$ on some interval (a, b) with $b \leqslant r_0$. In other words, the upper turning point is the same for different lower turning points and hence for different angular momenta; the corresponding rays cannot

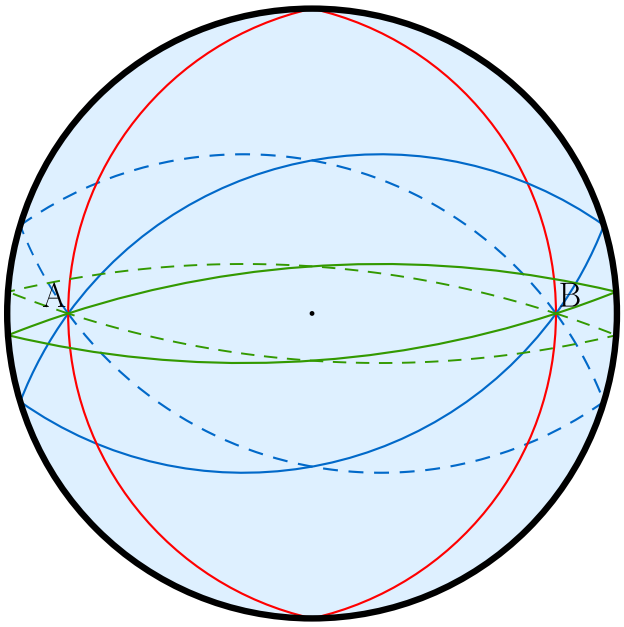

Figure 4. Ray trajectories in Maxwell's fish eye mirror.

get beyond $r = c$, which means reflection occurs at this point. Now there are two cases to be distinguished. In the first case $f(r) = c$ holds also for $0 \leqslant r < a$, which means that a reflection occurs for all rays that reach the point $r = c$; this corresponds to a perfect mirror placed at c. In the second case, the value $f(r)$ gets larger than c for some $r < a$. This means that rays with small angular momenta can penetrate beyond c; the reflection at c mentioned above must then be total internal reflection caused by a refractive index discontinuity at $r = c$. That such a discontinuity indeed exists follows from the fact that if $f(r) = c$ on the interval (a, b), then $f(r)$ must be discontinuous at $r = c$ and so must be $n(r)$ according to equation (18).

The discontinuity of the refractive index is normally connected with a partial reflection of the rays that do not undergo the total internal reflection. This would compromise the performance of the device because these partially reflected rays cannot contribute to the image. However, such a reflection can be eliminated by replacing the discontinuity by a smooth change of the index on the scale of a few wavelengths. Geometrical optics that we consider in this paper corresponds to the limit of $\lambda \to 0$, and so such a smoothing of the index is a negligible change and will not cause any considerable aberrations.

If the interval of constant f lies above r_0 then there will be a total reflection on a sphere 'from the outside'. This is illustrated in figure 6 where there is a mirror reflecting perfectly from the inside and a jump of refractive index reflecting totally some rays from the outside.

Spherical mirrors can be used to great advantage to reduce the size of the lens and also the range of the refractive index. An example is Maxwell's fish eye mirror discussed above that has equally good focusing properties as the original Maxwell's fish eye but its size is reduced from infinity to a unit disc (or sphere) and the refractive index range is reduced significantly from the interval $(0, 2]$ to just $[1, 2]$.

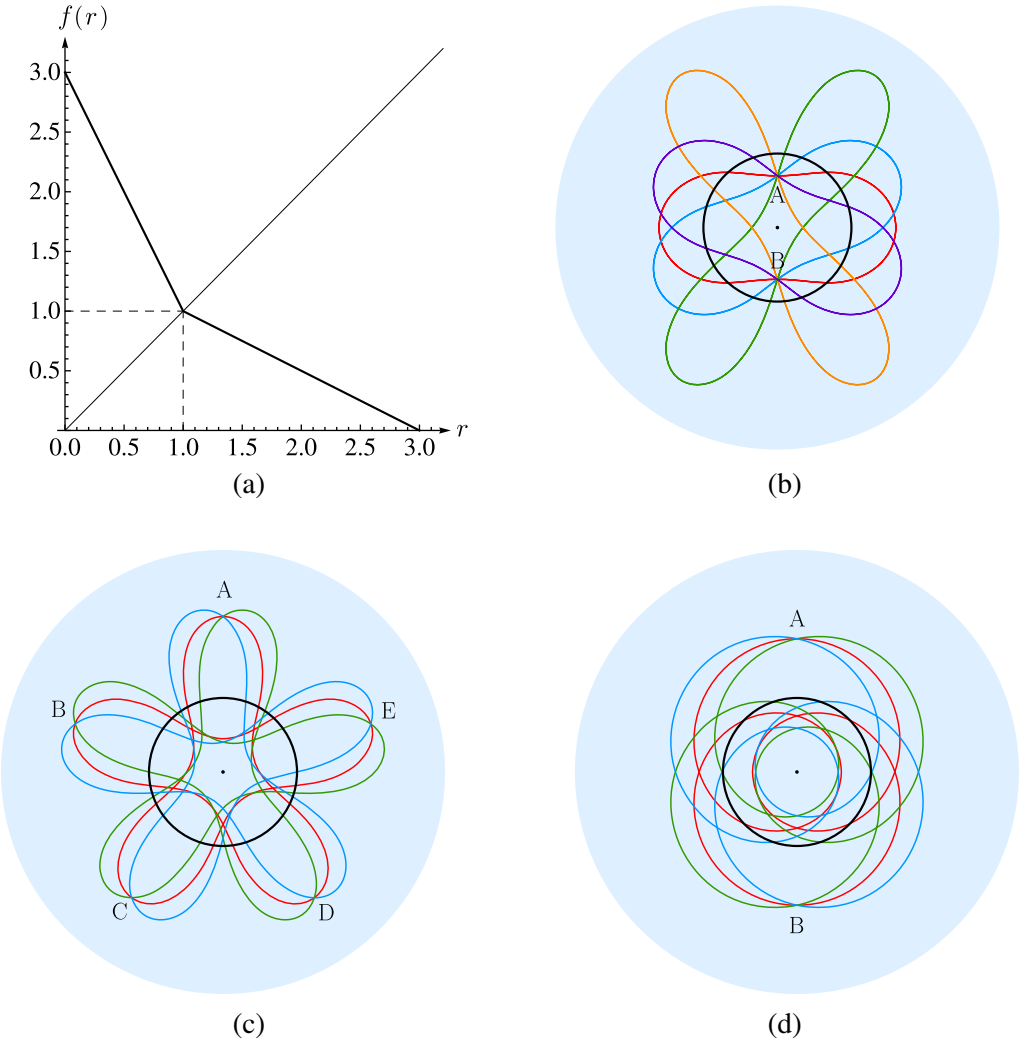

Figure 5. Graph of a sample function $f(r)$ according to equation (23) and the corresponding ray trajectories for (b) $m = 2$, (c) $m = 5/2$ and (d) $m = 2/3$. In (b) and (d), there is a strong image of A at B, while in (c) the images B, C, D, E of A are just weak.

6. Absolute instruments for homogeneous regions

In many absolute instruments such as Maxwell's fish eye, the optical medium fills the whole space and the object to be imaged must therefore be inserted into such an inhomogeneous medium. It is desirable to find optical devices that provide images of optically homogeneous spatial regions, i.e. regions with a uniform refractive index. Even if the refractive index of such a region differs from unity, this is still an advantage because one can fill this region with a suitable liquid and place the object in it.

Interestingly, until recently, the only known devices providing stigmatic images of optically homogeneous 3D regions were plane mirrors or their combinations [9]. This was changed by an excellent work of Miñano [18] who noticed that some well-known optical devices such as Eaton

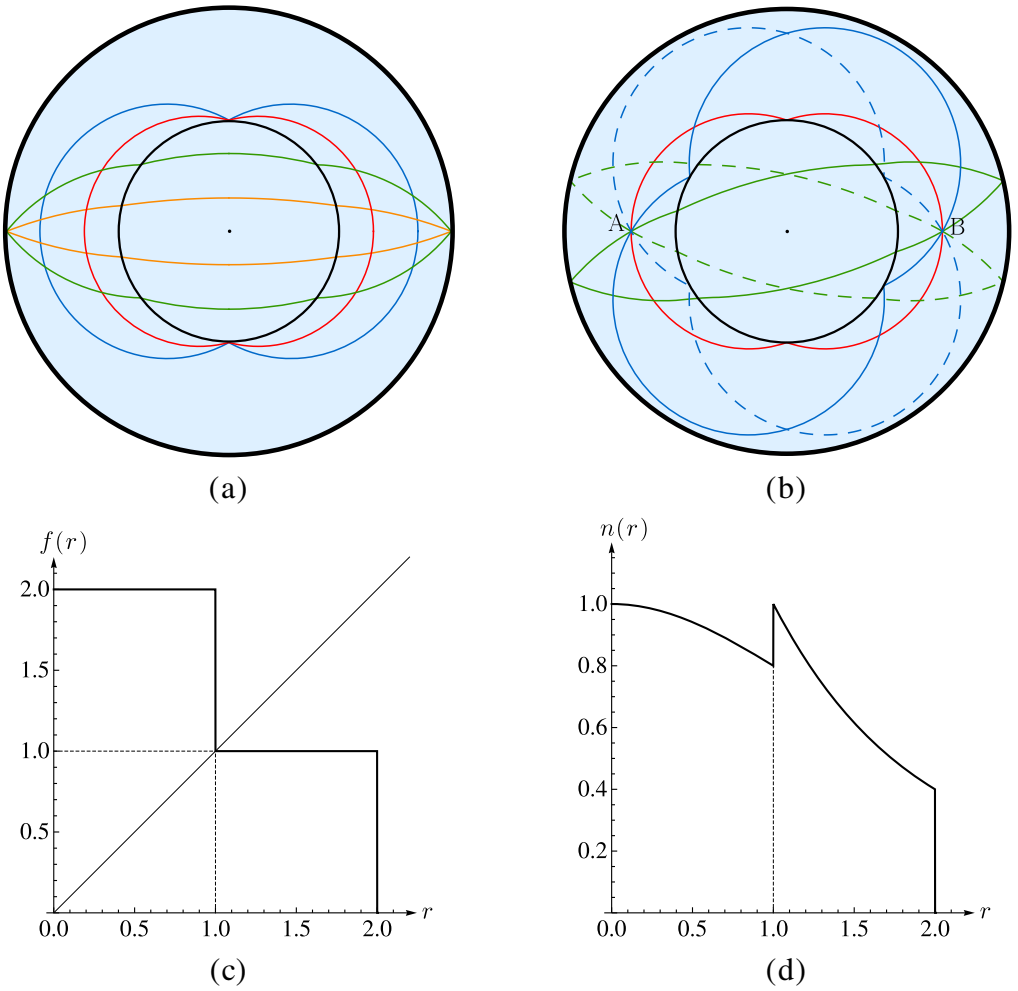

Figure 6. (a) Ray trajectories and (b) imaging by an absolute instrument with a spherical mirror at $r = 2$ and a jump of refractive index at radius $r = 1$. There are two types of ray trajectories differing by whether they do or do not penetrate inside the unit circle. (c) The corresponding function $f(r)$ and (d) refractive index.

or Luneburg lenses [13] are in fact absolute instruments, providing stigmatic virtual images. An even more important result of [18], however, is a device now called the Miñano lens that provides real images of homogeneous 3D regions.

6.1. Miñano lens

In the Miñano lens the homogeneous region is the unit disc with unit refractive index and the turning angle is $\Delta\varphi = \pi/2$, which corresponds to $m = 2$. To derive the refractive index outside the unit disc by our method, we will again use equation (18), but first we have to determine the function f. The lower turning point for a given L is simply $r_- = L$ because $n = 1$ in this region, the upper turning point is $r_+ = f(r_-)$. Substituting this into equation (14), we obtain a quadratic

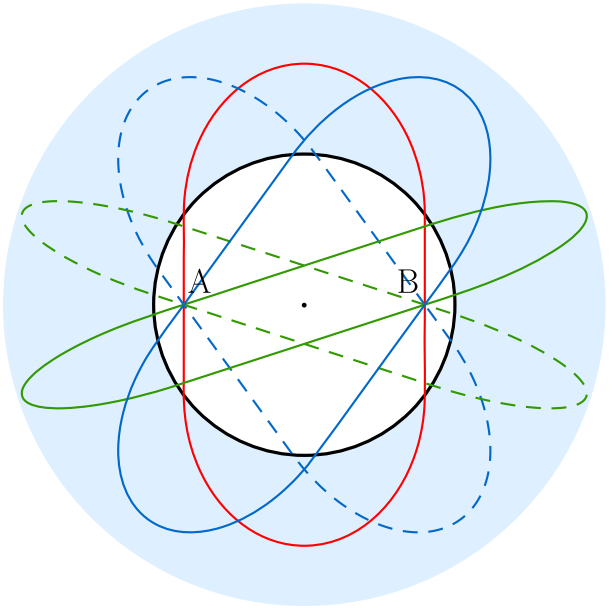

Figure 7. Ray trajectories in the Miñano lens. The optically homogeneous region is shown in white.

equation $f^2(r_-) - 2f(r_-) + r_-^2 = 0$ for $f(r_-)$ with the solution

$$r_+ = f(r_-) = 1 + \sqrt{1 - r_-^2} \tag{24}$$

(we have taken the larger root so that $r_+ \geqslant r_-$). Inverting this expression to obtain the function f also for r_+, we find $r_- = f(r_+) = \sqrt{2r_+ - r_+^2}$. Now we can combine equations (18) and (24) with $L_0 = 1$ to find the refractive index outside the unit disc. This gives precisely the expression (22), and so the refractive index of Miñano lens is

$$n(r) = \begin{cases} 1, & \text{for} \quad r \leqslant 1, \\ \sqrt{(2/r) - 1}, & \text{for} \quad r > 1, \end{cases} \tag{25}$$

and the ray trajectories are shown in figure 7.

6.2. Modified Miñano lens

Despite its elegance and nice properties, the Miñano lens has a disadvantage: its refractive index ranges from unity all the way to zero at $r = 2$, which is very difficult to realize practically. Since any refractive index profile can be multiplied by a real number without affecting the lens performance, we can define a measure of the index range as the ratio of its largest and smallest values

$$\eta \equiv n_{\max}/n_{\min}. \tag{26}$$

For the Miñano lens $\eta = \infty$. It would be very desirable to modify the lens somehow to make η finite. Fortunately, this is possible, as we will show now. Imagine we use the function f for $r < 1$ according to equation (24), but on the interval $[0, b]$ with $0 < b < 1$, we replace it by a constant value $c = 1 + \sqrt{1 - b^2}$. As we have seen, this corresponds to placing a mirror at $r = c$.

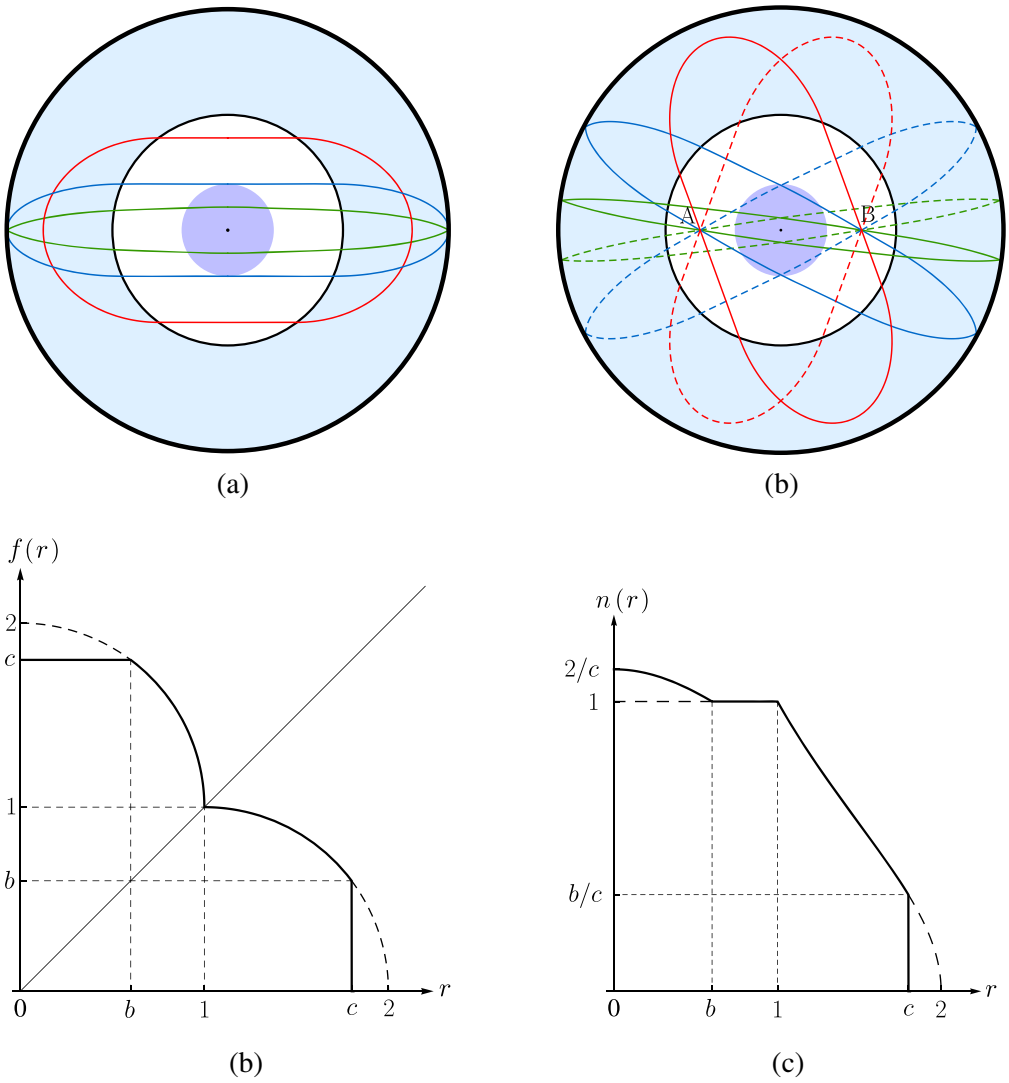

Figure 8. (a) Ray trajectories and (b) imaging by the modified Miñano lens. In contrast to the Miñano lens, there is a spherical mirror at radius c and an inner inhomogeneous region of radius b. (c) The corresponding function $f(r)$ and (d) refractive index $n(r)$. The dashed parts of the graphs on the intervals $[0, b]$ and $[c, 2]$ correspond to the original Miñano lens.

The function f in this way becomes

$$f(r) = \begin{cases} c, & \text{for} \quad r \leqslant b, \\ 1 + \sqrt{1 - r^2}, & \text{for} \quad b < r \leqslant 1, \\ \sqrt{2r - r^2}, & \text{for} \quad 1 < r \leqslant c, \end{cases} \tag{27}$$

see figure 8(c), and refractive index

$$n(r) = \begin{cases} 2c/\left(r^2 + c^2\right), & \text{for} \quad r \leqslant b, \\ 1, & \text{for} \quad b < r \leqslant 1, \\ \sqrt{2/r - 1}, & \text{for} \quad 1 < r \leqslant c, \end{cases} \tag{28}$$

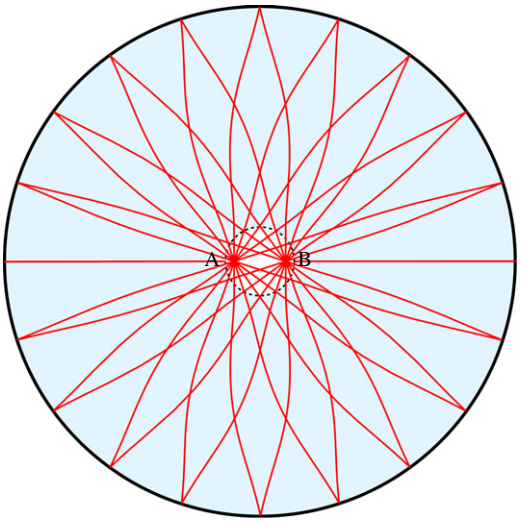

Figure 9. Rays in the lens imaging a spherical homogeneous region employing a spherical mirror. The homogeneous region is encircled by a dotted line. Unfortunately, the refractive index performing such an imaging perfectly does not exist as we show in the appendix.

see figure 8(d). We see that there appeared a region of radius b with Maxwell's fish eye index profile, which reduced the size of the homogeneous region. The largest and smallest values of the index occur at $r = 0$ and $r = c$, respectively, and yield the ratio $\eta = 2/b$. Choosing b not too small, one can obtain a very moderate index range of the lens; the price to pay is the reduction of the homogeneous region. Rays in a modified Miñano lens and its imaging properties are shown in figures 8(a) and (b).

6.3. A lens for designing a magnifying absolute instrument

Recently, we proposed another type of lens for imaging homogeneous spatial regions [19], which has a finite ratio of the largest and smallest refractive index. The homogeneous region is a unit sphere and there is a spherical mirror at radius $R > 1$. The refractive index between the two spheres is chosen such that a ray emerging in the direction of a unit vector $\vec{u}$ from a point A located at $\vec{r}_{\mathrm{A}}$ in the homogeneous region is incident on the mirror at the point $R\vec{u}$. This ensures that the ray after the reflection from the mirror passes through point B at $\vec{r}_{\mathrm{B}} = -\vec{r}_{\mathrm{A}}$ where an image of A is formed; see figure 9. Another property of the device is that, apparently, all mutually parallel rays propagating in the homogeneous region are focused to a single point at the mirror.

The refractive index calculated for this lens was based on the numerical solution of a specific integral equation that does not have an analytic solution. Unfortunately, it turned out later that the equation does not have solution at all, and so the proposed lens is in fact not an absolute instrument. The rays emerging from A hence do not pass exactly through B but there is some unavoidable aberration. However, numerical simulations reveal that this aberration can be very small if R is not too small. For this reason, the lens could have a practical importance, and we are therefore mentioning it here although it is not really an absolute instrument. The proof of non-existence of the solution of the integral equation is given in the appendix.

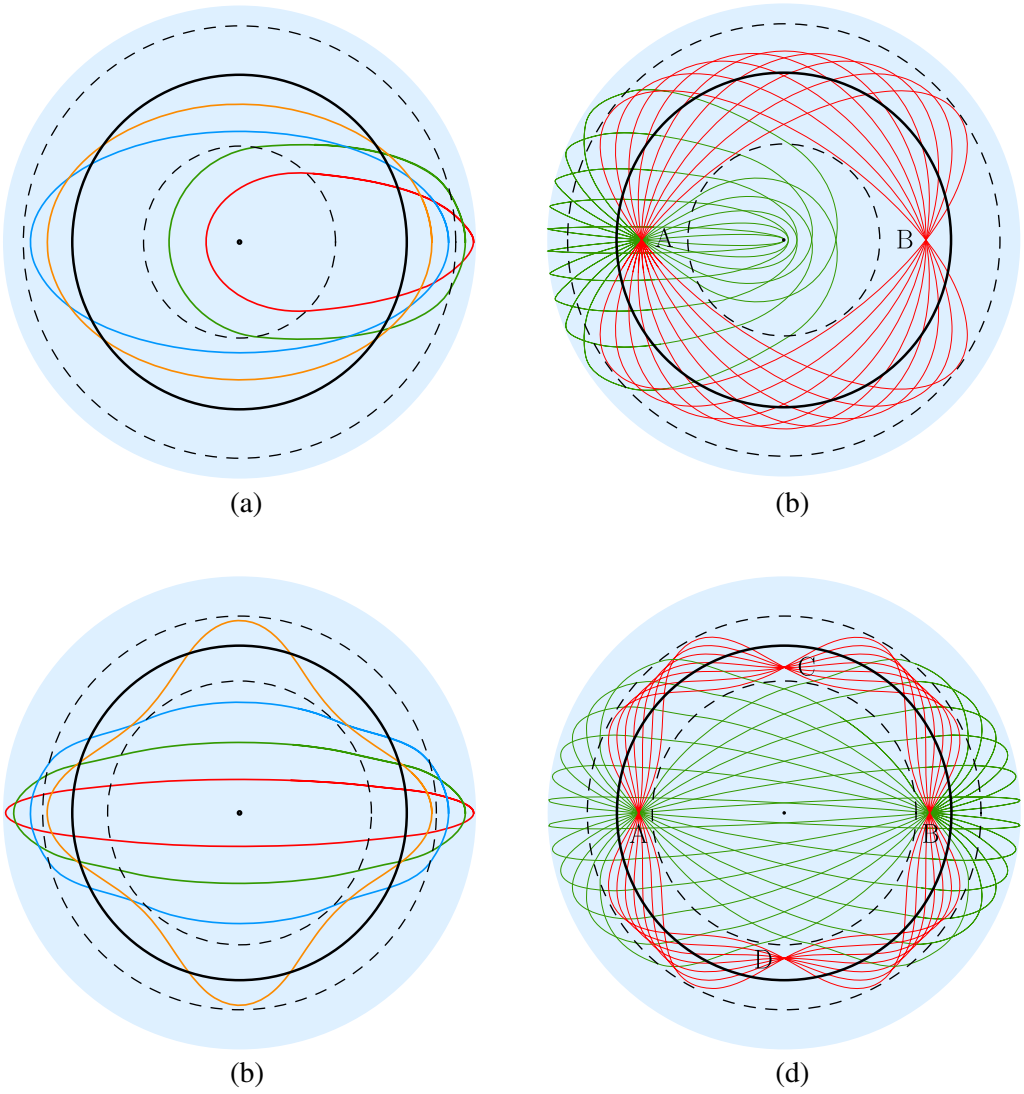

Figure 10. Ray trajectories in 'bifocal' lens with $L_0 = 1$, $L_1 = 3/4$, $f(r) = \sqrt{2a^2 - r^2}$ and (a, b) $m_1 = 1$, $m_2 = 2$ and (c, d) $m_1 = 2$, $m_2 = 4$. The dashed circles mark the radii of turning points corresponding to angular momentum L_1. Rays confined to the ring between these circles have turning angle $\Delta\varphi = \pi/m_2$ while rays that get outside the ring have $\Delta\varphi = \pi/m_1$.

7. Lenses with multiple image points

So far, we have considered just situations when the turning angle $\Delta\varphi(L)$ in equation (11) is constant for all angular momenta L from zero to L_0. However, another class of interesting absolute instruments can be obtained by taking $\Delta\varphi(L)$ piecewise constant on different intervals of L. In this situation, however, the refractive index cannot be found analytically with the help of equation (13) but must be calculated numerically. The simplest situation corresponds to two values of the turning angle: $\Delta\varphi(L) = \pi/m_1$ for $L \in [0, L_1]$ and $\Delta\varphi(L) = \pi/m_2$ for $L \in [L_1, L_0]$. Figures 10(a) and (b) show an example of this lens for $m_1 = 1$ and $m_2 = 2$. Rays

emerging from the point A with angular momentum larger than L_1 meet first at point B where they form an image and then continue back to A. On the other hand, rays with $L < L_1$ go back to A directly without passing through B. In this way, image B is formed just by some rays while image A is formed by all rays.

Since the transition from the first class of rays (those with $L > L_1$) to the second class ($L < L_1$) is not smooth, the optical path from A to B does not have to be the same for rays of the two types. In other words, the principle of equal optical path [9] does not apply to this type of lens.

Another example of such a 'bifocal lens' is shown in figures 10(c) and (d) for $m_1 = 2$ and $m_2 = 4$. In the 2D version of this problem, some rays emerging from A form an image at C or D and then continue to the image B. Other rays go to B directly without passing through C or D. If the lens is 3D, a strong image will be just at B (and then at A again), but weak images of A will be formed on the circle made by rotation of the points C and D about the axis AB. For coherent light waves emitted from the source at A, the inequality of the optical paths from A to B for the two ray types could lead to interesting diffraction patterns around the image point B if the two corresponding waves interfere destructively.

8. Conclusion

In this paper, we have derived a number of results for imaging by spherically symmetric absolute instruments. We have shown that images created by such instruments are either congruent with the object or related to it by spherical inversion. We have also proved that the mutual position of a point and its strong image is quite restricted in 3D: the straight line connecting the two points must intersect the centre of the lens.

Further, we have developed a general method for designing absolute instruments via solving the inverse problem for finite motion. We have shown how this method can be used for designing already known as well as a number of new absolute instruments. The modified Miñano lens we have proposed is particularly appealing because it produces a real stigmatic image of a homogeneous region with a reasonable range of refractive index, and we believe that this lens can find important practical applications. Whether the imaging devices discussed in this paper can provide super-resolution remains an open question, but in our opinion the answer is positive.

Acknowledgment

This work was supported by the grants MSM0021622409 and MSM0021622419 of the Czech Ministry of Education and by GAČR 202/08/H072.

Appendix. No-go theorem for spherically symmetric lenses

In the following, we show that the refractive index with the appealing properties described in section 6.3 does not exist. This gives a negative answer to the following question: is there a spherically symmetric medium that focuses parallel rays in a spherical cavity via a shell-shaped lens onto a single point? If the answer were positive, this would constitute a new interesting and practically important absolute instrument as well as a useful building block for other optical

devices [19]. Although the actual answer is negative by itself, it still useful and likely to influence future developments in the subject [20].

Consider parallel rays located in an inner spherical region $r \leqslant r_*$ with a constant refractive index $n_* \equiv \frac{N_*}{r_*} > 0$ that are focused by the medium to a point P situated at some finite distance $R > r_*$ from the centre O. We will try to determine an appropriate spherically symmetric profile $N(r) = rn(r)$ in the intermediate shell region

$$r_* \leqslant r \leqslant R \tag{A.1}$$

with inner and outer radii $r_* > 0$ and $R < \infty$, respectively. We will assume that all rays are outgoing, i.e. the radial position of a light ray $r(t)$ is monotonically increasing as a function of time t, and so no turning points are allowed. In particular, the outer region $r > R$ will play no role, and we might as well assume that the focal point P lies on the outer rim of the device. Suppose that the parallel rays move horizontally to the left and are focused to the focal point P with polar coordinates (R, π). As before, it is convenient to introduce the logarithm $x \equiv \ln r$ of the radial coordinate r. Similarly, we shall write $x_* \equiv \ln r_*$, $X \equiv \ln R$ etc in an obvious notation. Clearly N_* is the upper bound for the angular momentum L inside the inner region $r \leqslant r_*$. However, we shall only require that the focusing device actually works for rays with $L \in [0, L_m)$, where $L_m \in (0, N_*]$. A ray with angular momentum L emerges horizontally to the left from the inner rim at a polar angle $\pi - \arcsin \frac{L}{N_*}$ and when it arrives at P, the polar angle becomes π, and so the corresponding change of polar angle is $\arcsin \frac{L}{N_*}$. On the other hand, the same change can be calculated by integrating equation (10) from r_* to R, so we arrive at the following integral equation:

$$\forall L \in [0, L_m): \quad \frac{1}{L} \arcsin \frac{L}{N_*} = \int_{r_*}^{R} \frac{\mathrm{d}r}{r\sqrt{N^2(r) - L^2}} \equiv \int_{x_*}^{X} \frac{\mathrm{d}x}{\sqrt{N^2(x) - L^2}}. \tag{A.2}$$

We next redefine (normalize) the quantities $N' := \frac{N}{N_*}$, $L' := \frac{L}{N_*}$, $L'_m := \frac{L_m}{N_*}$, etc, by dividing with the constant N_*. Suppressing the primes from now on, we arrive at the main integral equation [19],

$$\boxed{\forall L \in [0, L_m): \quad \frac{\arcsin(L)}{L} = \int_{r_*}^{R} \frac{\mathrm{d}r}{r\sqrt{N^2(r) - L^2}} \equiv \int_{x_*}^{X} \frac{\mathrm{d}x}{\sqrt{N^2(x) - L^2}},} \tag{A.3}$$

which serves as our starting point. The solution function $N = N(r)$ is required to be bounded

$$\exists N_m \, \forall r \in [r_*, R]: \quad 0 < L_m \leqslant N(r) \leqslant N_m < \infty \tag{A.4}$$

for physical reasons, and Lebesgue measurable [21] in order for the integral (A.3) to be defined. Since the integrand (A.3) is non-negative, the integral is always defined, although perhaps infinite. The goal is now to investigate the integral equation (A.3), and show that it has no bounded solutions $N = N(r)$. Note that the kth moment $\int_{r_*}^{R} \frac{\mathrm{d}r}{r} \frac{1}{N^k(r)}$ is well defined and finite for any integer k because of the bounds (A.1) and (A.4).

Lemma A.1 (reformulation in terms of odd moments). *The integral equation (A.3) is equivalent to*

$$\boxed{\int_{r_*}^{R} \frac{\mathrm{d}r}{r} \frac{1}{N^{2n+1}} = \frac{1}{2n+1} \quad \text{for } n \in \mathbb{N}_0 \equiv \{0, 1, 2, 3, \ldots\}.} \tag{A.5}$$

Proof. The Taylor expansion of the $\arcsin(L)$ function at $L = 0$ is

$$\frac{\arcsin(L)}{L} = \sum_{n=0}^{\infty} \frac{1}{2n+1} \binom{2n}{n} \left(\frac{L}{2}\right)^{2n}. \tag{A.6}$$

On the right-hand side of equation (A.3), a binomial expansion produces

$$\begin{aligned}\int_{x_*}^{X} \frac{\mathrm{d}x}{\sqrt{N^2 - L^2}} &= \int_{x_*}^{X} \frac{\mathrm{d}x}{N} \left(1 - \left(\frac{L}{N}\right)^2\right)^{-1/2} = \int_{x_*}^{X} \frac{\mathrm{d}x}{N} \sum_{n=0}^{\infty} \binom{-1/2}{n} \left(-\left(\frac{L}{N}\right)^2\right)^n \\ &= \int_{x_*}^{X} \frac{\mathrm{d}x}{N} \sum_{n=0}^{\infty} \binom{2n}{n} \left(\frac{L}{2N}\right)^{2n} = \sum_{n=0}^{\infty} \binom{2n}{n} \int_{x_*}^{X} \frac{\mathrm{d}x}{N} \left(\frac{L}{2N}\right)^{2n}. \end{aligned} \tag{A.7}$$

In the last equality of equation (A.7), we were allowed to exchange integration and summation order, because each term is positive or zero (Tonelli's theorem). In the third equality of equation (A.7), we have used the identity

$$\binom{-1/2}{n} = \binom{2n}{n} \left(-\frac{1}{4}\right)^n. \tag{A.8}$$

Comparing the Taylor-coefficients on the left-hand side (A.6) and right-hand side (A.7) of equation (A.3) yields the reformulation (A.5).

□

Lemma A.2 (reformulation in terms of new L). *The integral equation (A.3) is equivalent to*

$$\boxed{\forall L \in \mathbb{C}: \ \mathrm{e}^{L^2} = \int_{r_*}^{R} \frac{\mathrm{d}r}{rN} \left(1 + 2\left(\frac{L}{N}\right)^2\right) \exp\left[\left(\frac{L}{N}\right)^2\right] \equiv \left(1 + \frac{\mathrm{d}}{\mathrm{d}\alpha}\right) \int_{r_*}^{R} \frac{\mathrm{d}r}{rN} \exp\left[\left(\frac{\alpha L}{N}\right)^2\right]\Bigg|_{\alpha=1}.} \tag{A.9}$$

Proof. The integrals in equation (A.9) are well defined due to the bounds (A.1) and (A.4). We calculate

$$\begin{aligned} L \int_{x_*}^{X} \frac{\mathrm{d}x}{N} \exp\left[\left(\frac{L}{N}\right)^2\right] &= L \int_{x_*}^{X} \frac{\mathrm{d}x}{N} \sum_{n=0}^{\infty} \frac{1}{n!} \left(\frac{L}{N}\right)^{2n} = \sum_{n=0}^{\infty} \frac{1}{n!} \int_{x_*}^{X} \mathrm{d}x \left(\frac{L}{N}\right)^{2n+1} \\ &\overset{(A.5)}{=} \sum_{n=0}^{\infty} \frac{1}{n!} \frac{L^{2n+1}}{2n+1} = \sum_{n=0}^{\infty} \frac{1}{n!} \int_0^L \mathrm{d}\ell \, \ell^{2n} = \int_0^L \mathrm{d}\ell \sum_{n=0}^{\infty} \frac{1}{n!} \ell^{2n} = \int_0^L \mathrm{d}\ell \, \mathrm{e}^{\ell^2}. \end{aligned} \tag{A.10}$$

In the second equality of equation (A.10), we use Tonelli's and Fubini's theorems [21] with x-independent majorant $\frac{|L|}{L_m} \exp[(\frac{|L|}{L_m})^2]$ to justify exchange of integration and summation order. Tonelli's and Fubini's theorems are also used in the fifth equality of equation (A.10) with majorant $\mathrm{e}^{|\ell|^2}$. Now differentiate both sides of equation (A.10) with respect to L to obtain equation (A.9). Note that equation (A.10) is trivially satisfied for $L = 0$, so we do not lose information when differentiating. Therefore, we can also run the argument backwards. □

Thus, we have three equivalent conditions, equations (A.3), (A.5) and (A.9), that a solution $N = N(r)$ should satisfy.

Lemma A.3. *If there exists a solution $N = N(r)$ (not necessarily monotonically increasing as a function of the radius r), then there also exists a monotonically increasing solution $\acute{N} = \acute{N}(r)$.*

Sketched proof: Lemma A.3 is basically the observation that the integration variable $x \equiv \ln r$ only enters implicitly via the function $N = N(x)$, and that the Lebesgue measure $\mathrm{d}x$ is translation invariant. □

From now on we can and we will make the following assumption A.4 without loss of generality.

Assumption A.4. *The solution $N = N(r)$ is a monotonically increasing function of r.*

At this point, we introduce a technical assumption A.5 in order to proceed.

Assumption A.5. *The inverse solution $r = r(N)$ exists and is differentiable with Lebesgue measurable derivative.*

Assumption A.5 implies that one can define a Lebesgue measurable density

$$\rho(N) := \frac{\mathrm{d}\ln r(N)}{\mathrm{d}\ln N} \geqslant 0. \tag{A.11}$$

Let us call the definition domain of the inverse solution $r = r(N)$ for $[N_*, N_m]$. In other words, $r(N_*) = r_*$ and $r(N_m) = R$.

Lemma A.6 (reformulation in terms of test functions). *Under the assumptions A.4–A.5, the integral equation (A.3) becomes equivalent to*

$$\boxed{\forall \eta \in C_c^\infty((0,\infty)) : \quad \int_{N_*}^{N_m} \rho(N)\mathrm{d}N\, \frac{\mathrm{d}\eta(N)}{\mathrm{d}N} = -\eta(1).} \tag{A.12}$$

Remark. Here $C_c^\infty((0,\infty))$ denotes the set of infinitely often differentiable functions η defined on the open interval $(0,\infty)$, and such that η has compact support in $(0,\infty)$. Compact support means that the function η is assumed to vanish identically in whole neighbourhoods around of $N = 0$ and $N = \infty$. It is therefore natural to extend η smoothly to the closed interval $[0,\infty]$ by assigning to η the values $\eta(0) = 0 = \eta(\infty)$ at the end points $N = 0$ and $N = \infty$.

Proof. When we substitute the inverse solution $r = r(N)$, equation (A.9) becomes

$$\mathrm{e}^{L^2} = \left(1 + \frac{\mathrm{d}}{\mathrm{d}\alpha}\right) \int_{N_*}^{N_m} \rho(N) \frac{\mathrm{d}N}{N^2} \exp\left[\left(\frac{\alpha L}{N}\right)^2\right]\Bigg|_{\alpha=1}. \tag{A.13}$$

Next perform the elementary substitution $\nu \equiv 1/N$ with limits $\nu_m \equiv 1/N_m$, and $\nu_* \equiv 1/N_*$. Furthermore, multiply both sides with $\mathrm{e}^{-(L\mu)^2}$, where $\mu > 0$ is a positive parameter. Then

$$\mathrm{e}^{L^2(1-\mu^2)} = \left(1 + \frac{\mathrm{d}}{\mathrm{d}\alpha}\right) \int_{\nu_m}^{\nu_*} \rho(\nu)\mathrm{d}\nu\, \mathrm{e}^{L^2((\alpha\nu)^2-\mu^2)}\Big|_{\alpha=1}. \tag{A.14}$$

Recall that the Dirac delta distribution $\delta(x)$ has the Fourier integral representation $\delta(x) = \int_{-\infty}^{\infty} \frac{\mathrm{d}p}{2\pi} \mathrm{e}^{\mathrm{i}px}$. By integrating $L^2 = \mathrm{i}p$ along the imaginary axis in equation (A.14), one obtains

$$\delta(1-\mu^2) = \left(1 + \frac{\mathrm{d}}{\mathrm{d}\alpha}\right) \int_{\nu_m}^{\nu_*} \rho(\nu)\mathrm{d}\nu\, \delta((\alpha\nu)^2 - \mu^2)\Big|_{\alpha=1}. \tag{A.15}$$

By using the Jacobian formula for the Dirac delta distribution

$$\delta(f(x)) = \sum_{x_i;\, f(x_i)=0} \frac{1}{|f'(x_i)|}\,\delta(x - x_i), \tag{A.16}$$

and multiplying both sides with 2, one obtains

$$\delta(\mu - 1) = \left(1 + \frac{\mathrm{d}}{\mathrm{d}\alpha}\right) \int_{\nu_m}^{\nu_*} \rho(\nu)\mathrm{d}\nu \frac{1}{\mu}\delta(\alpha\nu - \mu)\bigg|_{\alpha=1}, \tag{A.17}$$

where we have assumed that $\mu > 0$ is positive. Thus, for a test function $\eta \in C_c^\infty((0,\infty))$, one calculates

$$\begin{aligned}
\eta(1) &= \int_0^\infty \mathrm{d}\mu\ \eta(\mu)\delta(\mu - 1) \overset{(A.17)}{=} \left(1 + \frac{\mathrm{d}}{\mathrm{d}\alpha}\right) \int_{\nu_m}^{\nu_*} \rho(\nu)\mathrm{d}\nu \int_0^\infty \mathrm{d}\mu\ \frac{\eta(\mu)}{\mu}\delta(\alpha\nu - \mu)\bigg|_{\alpha=1} \\
&= \left(1 + \frac{\mathrm{d}}{\mathrm{d}\alpha}\right) \int_{\nu_m}^{\nu_*} \rho(\nu)\mathrm{d}\nu\ \frac{\eta(\alpha\nu)}{\alpha\nu}\bigg|_{\alpha=1} = \int_{\nu_m}^{\nu_*} \rho(\nu)\mathrm{d}\nu \left[\frac{\eta(\alpha\nu)}{\alpha\nu} - \frac{\eta(\alpha\nu)}{\alpha^2\nu} + \frac{\eta'(\alpha\nu)}{\alpha}\right]\bigg|_{\alpha=1} \\
&= \int_{\nu_m}^{\nu_*} \rho(\nu)\mathrm{d}\nu \frac{\mathrm{d}\eta(\nu)}{\mathrm{d}\nu}.
\end{aligned} \tag{A.18}$$

Now translate (A.18) back to the $N \equiv 1/\nu$ variable to obtain equation (A.12). □

Lemma A.7. *Equation (A.12) has no solutions for ρ that respects the bounds (A.4) on N.*

Proof. The fundamental lemma of calculus of variation (in the strengthened version of du Bois–Reymond) [22] shows that ρ must be a constant up to contributions that vanish almost everywhere. (In particular, we stress that it is not enough for ρ to be only piecewise constant.) Thus, one may pull the density ρ outside the integral (A.12), and integrate to obtain

$$\forall \eta \in C_c^\infty((0,\infty)): \quad \rho\,(\eta(N_m) - \eta(N_*)) = -\eta(1). \tag{A.19}$$

Collapsing limits $N_* = N_m$ are clearly not a solution. Assuming $N_* < N_m$, equation (A.19) has two solutions, $(\rho = 1, N_* = 1, N_m = \infty)$, or $(\rho = -1, N_* = 0, N_m = 1)$. However, neither of these two solutions respect the bounds (A.4) on N, and the latter is actually monotonically decreasing. □

References

[1] Pendry J B 2000 *Phys. Rev. Lett.* **85** 3966
[2] Soukoulis C M, Linden S and Wegener M 2007 *Science* **315** 47
[3] Fang N *et al* 2005 *Science* **308** 534
[4] Stockman M I 2007 *Phys. Rev. Lett.* **98** 177404
[5] Leonhardt U 2009 *New J. Phys.* **11** 093040
[6] Leonhardt U and Philbin T G 2010 *Phys. Rev.* A **81** 011804
[7] Ma Y G *et al* 2011 *New J. Phys.* **13** 033016
[8] Maxwell J C 1854 *Camb. Dublin Math. J.* **8** 188
[9] Born M and Wolf E 2006 *Principles of Optics* (Cambridge: Cambridge University Press)
[10] Hendi A, Henn J and Leonhardt U 2006 *Phys. Rev. Lett.* **97** 073902
[11] Leonhardt U and Philbin T 2010 *Geometry and Light: The Science of Invisibility* (New York: Dover)
[12] Firsov O B 1953 *Zh. Eksp. Teor. Fiz.* **24** 279

[13] Luneburg R K 1964 *Mathematical Theory of Optics* (Berkeley, CA: University of California Press)
[14] Ostrovsky V N 1997 *Phys. Rev.* A **56** 526
[15] Landau L D and Lifshitz E M 1976 *Mechanics* (Oxford: Butterworth-Heinemann)
[16] Demkov Y N and Ostrovsky V N 1971 *Sov. Phys.—JETP* **33** 1083
[17] Eaton J E 1952 *Trans. IRE Antennas Propag.* **4** 66
[18] Miñano J C 2006 *Opt. Express* **14** 9627
[19] Tyc T and Šarbort M 2010 arXiv:1010.3178
[20] Tyc T 2011 arXiv:1103.3406
[21] Rudin W 1966 *Real and Complex Analysis* (New York: McGraw-Hill)
[22] Hörmander L 1990 *The Analysis of Linear Partial Differential Operators I: Distribution Theory and Fourier Analysis* (Berlin: Springer)